Journal of
Materials Chemistry A

ROYAL SOCIETY
OF CHEMISTRY

PAPER

View Article Online
View Journal | View Issue

Cite this: *J. Mater. Chem. A*, 2023, **11**, 20187

Boosting the rate performance of primary Li/CF$_x$ batteries through interlayer conductive network engineering†

Fan Zhang,‡[a] Yingying Lan,‡[a] Renjie Li,[a] Jianlin Wang,[b] Shengxiang Wu,[a] Lejuan Cai,[a] Yu Zhao[b] and Wenlong Wang *[abc]

Received 12th July 2023
Accepted 25th August 2023

DOI: 10.1039/d3ta04102f

rsc.li/materials-a

As an attractive cathode material with an ultra-high theoretical capacity and energy density, graphite fluoride (CF$_x$) is a promising option for lithium primary batteries. However, its application in high-power-demanding scenarios is limited by its poor rate performance, mainly due to its intrinsic low electrical conductivity and sluggish electrochemical kinetics. Herein, we demonstrate an innovative method that could improve the electron-transport properties and electrochemical kinetics of CF$_x$ simultaneously. This was achieved by exfoliating CF$_x$ into quasi-2D flakes and constructing conductive networks within the interlayers. The strong electronic interaction between CF$_x$ and the conductive network enabled facile charge transfer, as reflected by photoluminescence quenching and electrochemical characterization tests. This newly designed CF$_x$ cathode outperformed conventional ones in a lithium primary battery, delivering a specific capacity of 580 mA h g^{-1} at a high discharge rate of 2C, which was 77% of the charge capacity at 0.1C.

Introduction

The lithium/fluorinated carbon (Li/CF$_x$)-based primary battery, developed by Watanabe *et al.* and available from the Matsushita Electric Industrial Company since 1970s,[1–3] is a promising route toward high-energy-density devices. With a high and stable discharge platform, large capacity, excellent shelf-life with capacity losses of only 0.5% per year and other advantages, Li/CF$_x$ batteries have been widely applied in medical devices and aerospace equipment.[2] However, at a fast discharge rate, the Li/CF$_x$ battery can hardly reach its theoretical capacity (865 mA h g^{-1}, $x = 1$ for CF$_x$) or operate without sacrificing plateau voltages (open-circuit voltage of 3.1–3.6 V).[4,5] This is due to the intrinsic low electrical conductivity of CF$_x$ and the impedance of lithium-ion insertion into CF$_x$ layers,[6] which in turn lead to electrochemical polarization and deterioration of the rate performance.[7–9]

It is widely acknowledged that CF$_x$ suffers from a poor conductivity if x is close or greater than 1, which originates from the ionic or covalent nature of the C–F bond.[10,11] Several methods have been employed to tackle this problem; for instance, coating conducting additives, *e.g.*, carbon from any sources,[12] or polymers such as polypyrrole and PANI[13,14] on the CF$_x$ particles to form surface conductive layers. Another alternative strategy is to utilize sub-fluorinated CF$_x$ ($x < 1$),[15] wherein the reduced fluorine–carbon ratio indicates the presence of sp^2 carbon, which serves as a facile electron-transport path. Additionally, low-dimensional CF$_x$, such as nano CF$_x$ synthesized from different precursors, *e.g.*, carbon nanotubes, carbon nanoflakes, and reduced graphene oxide (RGO),[5,16–20] is also a great way to mitigate the conductivity issue. The low-dimensional CF$_x$ not only provides a large specific surface area and shortens the diffusion distance of lithium ions, but also facilitates electron transfer due to an intentional or unintentional defluorination effect. While these approaches have been successful regarding the overall performances of Li/CF$_x$ batteries, overcoming the intrinsic conductivity bottleneck of the CF$_x$ cathode at a submicron scale remains a challenge.

In this work, we demonstrate a novel CF$_x$ cathode design that includes single-walled carbon nanotubes (SWCNT) between layers of exfoliated CF$_x$ (Fig. 1a). The cathode design serves two important roles: (a) it improves the electron-transport rate and (b) promotes the electrochemical kinetics because of the enlarged interlayer distances. We should emphasize here that the SWCNTs in this work were not simply "additives" or "coating layers" that facilitate charge transfer dictated in Ohm's law;[8,21] instead, they formed channels for both electrons and ions transportation. By utilizing high-spatial-resolution optical

---

[a] *Songshan Lake Materials Laboratory, Dongguan, Guangdong 523808, China*

[b] *State Key Laboratory for Surface Physics, Beijing National Laboratory for Condensed Matter Physics, Institute of Physics, Chinese Academy of Sciences, Beijing 100190, China. E-mail: wwl@iphy.ac.cn*

[c] *School of Physical Sciences, University of Chinese Academy of Sciences, Chinese Academy of Sciences, Beijing 100190, China*

† Electronic supplementary information (ESI) available. See DOI: https://doi.org/10.1039/d3ta04102f

‡ These authors contributed equally to the work.

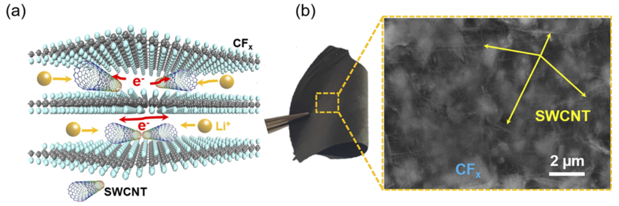

Fig. 1 (a) Schematic diagram of the CF_x/SWCNT cathode. (b) Optical and SEM image of the CF_x/SWCNT film.

spectroscopy, we confirmed the rapid charge transfer between SWCNT and CF_x at the micrometre scale. Furthermore, based on the newly designed CF_x cathode, an as-fabricated Li/CF_x primary battery performed well, with an excellent power density, delivering 675 and 580 mA h g^{-1} at 1C and 2C high discharge rates.

Experimental section

CF_x electrode fabrication

CF_x (x ranging from 0.9 to 1, as determined by EDX, XFNANO Materials Tech Co., Ltd) was investigated as the active cathode material in Li/CF_x batteries. First, 15 mg CF_x, 3 mg SWCNT, and 300 mL *n*-methylpyrrolidone (NMP) were stirred and dispersed by an ultrasonic homogenizer at 260 W for 20 min. The exfoliation of CF_x takes place during this stage. The mixed solution was then pumped and filtered through a microporous filter membrane (with a diameter of 4.7 cm and a pore diameter of 0.45 μm), and deposited as a self-supported hybrid film. To improve the conductivity, 1 mg SWCNT was deposited on this film following the same procedure. After drying in the oven at 80 °C to remove the residual solvent, the resulting film was cut into small discs with a diameter of 1 cm. Then, these were pressed on titanium mesh as a current collector, forming a working cathode.

For comparison, the same CF_x, Super P as a conductive additive, and poly (vinylidene fluoride) (PVDF) as a binder were mixed in NMP with an 8 : 1 : 1 weight ratio, following conventional recipes.[22,23] The CF_x electrode film was prepared by coating slurries on pre-cleaned Al foil. Then, shaped electrode pieces were further dried at 80 °C under vacuum for at least 12 h. The loading of the active materials was about 1–2 mg for each electrode. Finally, both films were transferred to a glovebox for Li coin cell assembly.

Electrochemical measurements

The Li/CF_x coin cells were assembled in an argon-filled glovebox (H_2O < 0.1 ppm, O_2 < 1 ppm) with electrolytes (1 M $LiPF_6$ with an EC : DMC ratio of 1 : 1). The coin cells were discharged under different current densities from 0.1C to 2C for each electrode on a Neware Battery Test System (Neware Technology Limited, Shenzhen, China) with a termination discharge voltage of 1.5 V. Electrochemical impedance spectroscopy measurements were carried out on an electrochemical workstation (CHI 760E from CH Instruments, Inc.) in the frequency range between 10 kHz and 200 mHz with a voltage amplitude of 5 mV. Galvanostatic intermittent titration technique (GITT) experiments were carried out using the Neware Battery Testing System. The assembled Li/CF_x cell was discharged at a 0.1C rate for 10 min followed by a relaxation time interval of 20 min, and this procedure was repeated until the voltage reached 1.5 V.

Optical characterization

Photoluminescence and Raman measurements were conducted with a Horiba LabRam HR Evolution confocal Raman microscope with a 600 g mm^{-1} grating and 633 and 532 nm lasers as the excitation source. Data were taken using a 50× (NA = 0.5) microscope lens. For the 325 nm laser, a 15× (NA = 0.31) NUV lens was applied. Before measurement, the CF_x samples were heated at 80 °C in a vacuum to remove any possible solvent residue. All the measurements were performed at room temperature under ambient conditions. Each spectrum shown in the main text and ESI† is representative of at least 8 different locations on the sample surface.

Results and discussion

Design of the CF_x/SWCNT cathode

To improve the electron-transport rate of the CF_x cathode as much as we could, bulk CF_x was exfoliated first, together with monodispersed SWCNT insertion into the CF_x flakes (Fig. 1a, details of the fabrication process are given in the Experimental section). High-resolution SEM imaging was used to provide morphology information of this self-supported hybrid CF_x film (Fig. 1b), indicating a conductive network was formed in the CF_x matrix. In this work, CF_x could be dispersed as quasi-2D flakes (Fig. S1a†), so the SWCNTs could be easily "inserted" into the CF_x interlayers in the final fabricated film (Fig. S1b†), which improved the conductivity significantly. Here, the CF_x was considered as exfoliated two-dimensional layers instead of a bulk material, so the SWCNT networks could go between the CF_x layers. This design offers several advantages over cathodes made from slurries by simply mixing CF_x and SWCNTs, in which SWCNTs can easily aggregate (Fig. S1d†).

In order to test whether the conductive network in the CF_x/SWCNT cathode was effective, we needed to make sure the charge transfer was locally optimized. However, conventional electrical or electrochemical characterization methods can only probe the charge-transfer rate/efficiency at the macroscopic scale, while microscopic information and detailed mechanism are missing. Therefore, confocal microscopy was employed in this work to provide microscopic electrical conductivity information at a resolution of ~1 μm.

Rapid charge transfer between CF_x and SWCNT

The photoluminescence (PL) of the exfoliated CF_x and CF_x/SWCNT film was measured at different excitation wavelengths. Fig. 2a shows the PL spectra of the exfoliated CF_x under 633 and 532 nm excitation, where strong and broad PL peaks centred at 705 nm could be observed in both cases. Also, shoulder peaks appeared at 652 and 590 nm for the 633 and 532 nm excitation

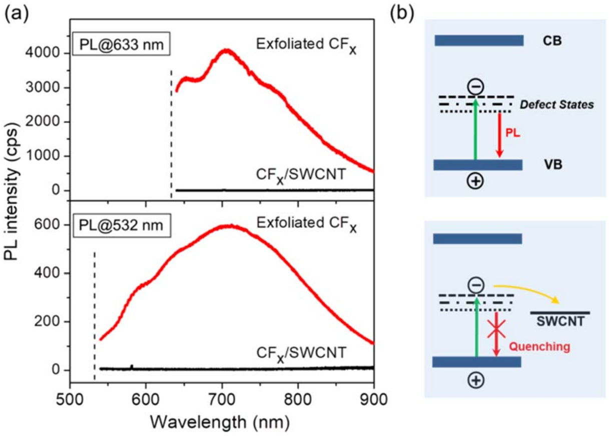

Fig. 2 (a) PL spectra of exfoliated CF$_x$ and CF$_x$/SWCNT with 633 and 532 nm lasers under 0.68 and 0.32 kW cm^{-2} excitation. Amplification of the CF$_x$/SWCNT spectra is shown in the ESI.† Vertical dashed line represents the laser wavelength. (b) Scheme of the fluorescence process and charge transfer between CF$_x$ and SWCNT. Green arrows represent the slight visible-light absorption related to defects.

conditions, respectively. The laser excitation energy (1.96, 2.33 eV) and 1.76 eV peak energy (705 nm) were much lower than the estimated band gap value of CF$_x$ (x = 1), which is at least 3.1 eV.[11] If CF$_x$ was similar to intrinsic semiconductors, like silicon or GaAs, then electronic transition would be impossible. As a result, it is unlikely that the strong PL that can be seen in Fig. 2a was from band edge emission. Actually, the broad peak suggests that electronic transition was between defects and the conduction or valence band.[24] Fig. S2† shows the PL spectrum of the exfoliated CF$_x$ under a 325 nm laser. With a 3.8 eV high excitation energy, a broad PL spectrum can still be observed, while the obtained peak energy (2.21 eV) was different from that at a lower energy excitation, suggesting various kinds of defects within the exfoliated CF$_x$. Similar to carbon dots and reduced graphene oxide, CF$_x$ has abundant mid-gap states, which substantially enhance the luminescence through recombination between the conduction band (or valence band) and defect levels (Fig. 2b).[25,26] During the exfoliation process, a slight surface defluorination, together with sp^2 and sp^3 carbon rearrangement, unavoidably takes place on the surfaces of CF$_x$ particles,[22,27] leading to a stronger background PL.

When the exfoliated CF$_x$ was mixed with monodispersed SWCNTs, the background PL of CF$_x$/SWCNT was zero, or close to zero in most spots we tested (flat lines in Fig. 2a, S2, and S3,† under 633 to 325 nm wavelength excitation), exhibiting a significant difference from the case of exfoliated CF$_x$. As shown in these figures, only the Raman signals from SWCNT and CF$_x$ were observed.[28] Here the SWCNTs formed conductive networks within the 2D layers (Fig. 1b and S1b†), not like the additives in the Super P sample (Fig. S1c†). As a result, the PL quenching of the exfoliated CF$_x$ was attributed to the distinguished electronic interaction between CF$_x$ and SWCNT, instead of a light-blocking effect.

The link between the PL quenching and electron transport can be understood as follows. As shown in Fig. 2b, excited carriers in CF$_x$ can be created by photoexcitation or injection from the outer electrical circuit. No matter which kind, they will eventually recombine to the ground state, mainly through the defects. During the transition process, luminescence was observed (Fig. 2a and S2a†). For the trapped electrons, their mobility, and thus the conductivity of the film, is limited by the scattering effects with defects, disordering, and other factors.[29,30] While in CF$_x$ primary batteries, a higher conductivity of the cathode material is beneficial for device performance, and any trapped carrier is unwanted. Therefore, complete PL quenching in this case suggests that even the carriers trapped in defects can be extracted. In the literature, similar PL quenching experiments as above are normally performed with an additional electron or hole extraction layer for photovoltaic materials, like in the newly emerged hybrid perovskites, to illustrate a fast photoexcited charge-transfer rate.[31] However, usually PL intensity reduction instead of quenching has been observed,[32,33] due to bulk carrier localization or a poor interfacial electrical contact. Therefore, the nearly complete PL quenching of CF$_x$/SWCNT suggests a stronger electronic interaction between the additive (SWCNT) and host (CF$_x$) in this work.

In reality, for the exfoliated CF$_x$, the sp^2 carbon produced within the fabrication processes helps carrier transportation or extraction to some extent, but not enough to quench the PL as the CF$_x$ flakes are isolated from each other; rather it is the SWCNTs bridging these flakes and facilitating charge transfer that eventually lead to the complete quenching of the PL. For accuracy we performed the same measurement microscopically using confocal microscopy to ensure good electrical contact was maintained throughout the CF$_x$/SWCNT. This argument was also used in the optimization of the CF$_x$ cathodes.

Electrochemical performance of the CF$_x$/SWCNT cathode

Coin cells with a metallic lithium counter electrode were tested to evaluate the newly designed cathode's performance (Fig. 3). The CF$_x$/SWCNT cathode showed an improved rate performance, especially at 1C and 2C discharge rates (Fig. 3a), compared to the conventional ones with Super P as the conductive additive. For example, the specific capacity at the discharge rate of 2C was 580 mA h g^{-1}, which was an impressive 77% of the level under the 0.1C rate, and the plateau voltage was maintained at 2.1 V. Moreover, the cathode based on the SWCNT network showed little voltage delay, verifying the

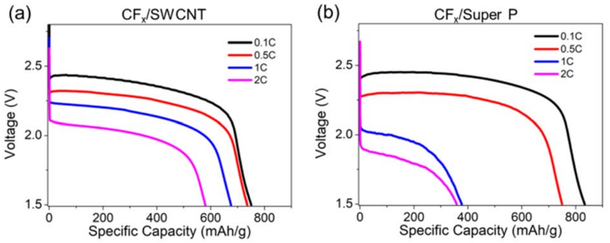

Fig. 3 Galvanostatic charge–discharge (GCD) curves of a Li/CF$_x$ battery based on the SWCNT cathode (a) and on a Super P cathode (b) under different discharge rates.

improved electronic conductivity of the active CF_x particles at the initial stage of discharge. Meanwhile, the Super P cathode delivered a discharge capacity of 830 mA h g^{-1} at 0.1C, approaching the theoretical value of 865 mA h g^{-1} for CF_x (x = 1), with the plateau voltage of 2.4 V (Fig. 3b). At high discharge rates of 1C and 2C, although an optimized ratio (10 wt%) of Super P was applied to improve the conductivity, the CF_x cathode without the SWCNT conductive network still showed inferior electrochemical performance. At the 2C discharge rate, the capacity was reduced to ~400 mA h g^{-1} and the operating voltage was below 1.9 V.

The rate performance of the CF_x/Super P cathode, defined here as the capacity ratio between the performance at 2C and 0.1C, was consistent with the PL measurements discussed above. For nearly insulating CF_x,[6] complete PL quenching or effective electron conduction was difficult, even with the optimized ratio of Super P additives. The observed rate performance enhancement of the CF_x/SWCNT cathode could not be simply attributed to the higher weight ratio of conductive "additive". For instance, we fabricated a CF_x cathode with 10% SWCNTs incorporated as conductive networks (Fig. S4†). With a similar weight ratio of conductive agent as the CF_x/Super P sample, the specific capacity of this cathode at the discharge rate of 2C still maintained 73% of the level under the 0.1C rate. These results suggest the need to pay more attention to the interaction between the conductive agent and CF_x than to the ratio of certain components.

We note here that the specific capacity of the CF_x/SWCNT cathodes at 0.1C was 750 mA h g^{-1}, which was lower than for the Super P counterpart (830 mA h g^{-1}). The slightly declined capacities of the CF_x/SWCNT cathode at 0.1C may be related to surface defluorination,[22] as confirmed by the PL characteristics of the exfoliated CF_x and the EDX results (Table S1†). However, over 90% capacities were maintained, suggesting only a slight degree of defluorination. After all, the C–F bonds in CF_x are semi-ionic and covalent,[4,34] which can hardly be broken during our fabrication processes.

To confirm the influence of the conductive network and layered structure on the electrochemical performance, electrochemical impedance spectroscopy (EIS) was carried out at the initial and end stages of the discharge process, and the difference in electrochemical performance was explored (Fig. 4). In the equivalent circuit model,[35] the symbols R_1, R_{ct}, W_1, and C denote the ohmic resistance, charge-transfer resistance, Warburg impedance (Ws-R as the diffusion impedance), and double-layer capacitance, respectively. The fitting results of R_1, R_{ct}, and Ws-R are listed in Table 1. Comparing Fig. 4a and b, it can be seen that the SWCNT conductive network within the CF_x flakes led to a significantly lower ohmic resistance (~29 Ω *versus* over 41 Ω). For R_{ct}, CF_x/SWCNT showed a smaller value before discharge (3454 Ω *vs.* 4337 Ω), implying faster lithium-ion diffusion and reaction kinetics. The huge difference in ion-diffusion impedance (Ws-R, Table 1, 56.0 Ω *vs.* 604.1 Ω) between the two cathodes further proved that the effective diffusion barrier was lowered because of CF_x layer exfoliation and SWCNT intercalation.

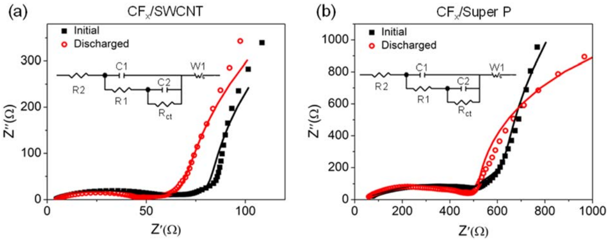

Fig. 4 Nyquist plots of the electrochemical impedance spectra, measured for Li/CF_x batteries based on the SWCNT (a) and Super P cathode (b) before and after discharge at 1C, together with the fitting model.

As a requirement for charge balance for faradaic electrochemical reactions, electron transfer and ion movement are coupled with each other. Therefore, the better electron transfer rate confirmed above was also responsible for the enhanced electrochemical kinetics. In Wang's previous work,[36] *in situ* TEM experiments were performed and showed an abrupt switch from a high-resistance to low-resistance state for a single CF_x particle during discharge. The observed electrical resistance decrease was accompanied by easier lithium-ion intercalation into the CF_x interlayer, together with carbon generation during discharge. For the CF_x/SWCNT cathode in this work, the conductive matrix instead of reaction-produced carbon provides a facile electron pathway. Also, the quasi-2D structure of exfoliated CF_x is beneficial for lithium-ion transportation, as evidenced by comparison of the EIS parameters between the two cathodes in Table 1. Therefore, the design of CF_x/SWCNT improved the coupling between electrons and ions, and thus led to the better electrochemical performance.

Moreover, the CF_x/SWCNT hybrid cathode showed little differences in R_1, R_{ct}, and Ws-R before and after discharge, while an obvious variance in CF_x/Super P could be observed from the fitted EIS parameters in Table 1 and Fig. 4b. Similar to the mechanism unveiled in ref. 36, we rationalize this phenomena as follows. Carbon and LiF are continuously produced in the CF_x/Super P composite. Especially at the beginning of discharge, CF_x relies on the carbon to transport electrons, which causes voltage delay. The overall electrical conductivity changes rapidly in this case, together with a large variance in the ion-diffusion barrier due to possible diffusion channel blockage. While for CF_x/SWCNT, the conductive network exists at the initial stage, and the charge transfer is fast all the time, which explains its good performance under high discharge rates in Fig. 3a.

To reveal the advantage of the CF_x/SWCNT design more clearly, we measured the diffusion coefficient D_{Li^+} between CF_x

Table 1 Selected fitting parameters of the EIS model in Fig. 4

Cathode	R_1 (Ω)	R_{ct} (Ω)	Ws-R (Ω)
CF_x/SWCNT initial	29.4	3454	56.0
CF_x/SWCNT discharged	26.9	3412	55.9
CF_x/Super P initial	41.0	4337	604.1
CF_x/Super P discharged	85.0	2118	447.6

layers by the galvanostatic intermittent titration technique (GITT) method (Fig. 5a–d). During the GITT measurement, the cell was discharged with a constant current density of 0.1C for an interval of 10 min, followed by 20 min relaxation to get the steady-state voltage E_s, until the voltage was below 1.5 V. The resulting voltage profile for a single titration at the plateau voltage during the discharge process is shown in Fig. 5b with the parameters labelled. Meanwhile, Fig. 5c shows the plot of voltage *vs.* $t^{1/2}$ recorded for both cathodes, indicating a roughly linear relationship in the time domain from 10 to 100 s. Then, D_{Li^+} was calculated from eqn (1), where the average radius of CF_x particles R_s was determined from the SEM images.[37]

$$D_{\mathrm{Li}^+} = \frac{4}{\pi\tau}\left(\frac{R_s}{3}\right)^2\left(\frac{\Delta E_s}{\Delta E_t}\right)^2 \quad (1)$$

The D_{Li^+} for both CF_x cathodes fell in the range from $\sim 10^{-14}$ to $\sim 10^{-11}$ cm^2 s^{-1} (Fig. 5d), which is the same order of magnitude as the values in the literature.[7,38] The D_{Li^+} values of the two samples were almost equivalent at the beginning of the discharge state. In this region, C–F bond consumption, LiF growth, and carbon generation have profound and complex influences on the ion-diffusion kinetics. In the deep discharged state, CF_x/SWCNT possessed a higher D_{Li^+} than that of the CF_x/Super P cathode, especially in the potential under 2.0 V. Here, too much non-conducting LiF generation leads to a partial blockage of ion diffusion, together with the decay of D_{Li^+} after the maximum value.[6] Note that the D_{Li^+} is the diffusion coefficient in layered or bulk CF_x materials according to its definition,[39] which is related to but different from the Ws-R in EIS measurements. The higher D_{Li^+} values of the CF_x/SWCNT sample originated from the 2D nature of the CF_x flakes, indicating better coupling between electron transfer and Li^+ transportation within the interlayers.

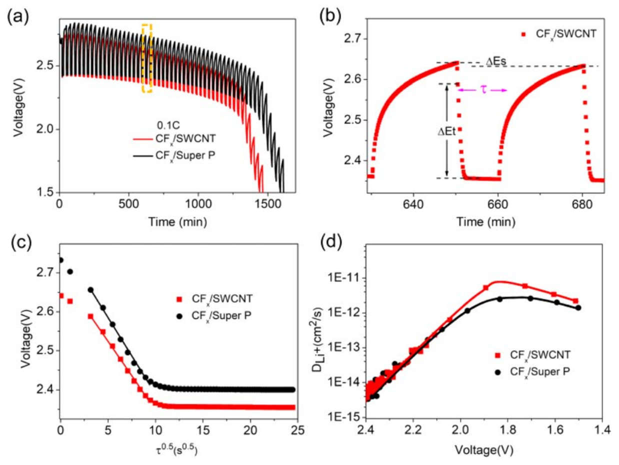

Fig. 5 (a) GITT curve of Li/CF_x batteries at 0.1C. (b) Scheme for a single step of a GITT experiment in the yellow region in (a). (c) Linear behaviour of the transient voltage changes against $\tau^{1/2}$ during a single titration process. (d) Derived lithium diffusion coefficient of the two cathodes at 0.1C. Plotted line is for eye guidance.

The above analyses indicate that the sluggish charge transfer in bulk CF_x and slow ion diffusion are the main reasons for the poor electrochemical performance of the conventional CF_x cathode at high discharge rates. During the discharge process, the generated sp^2 carbon might transport charges well, but the nonconductive LiF accompanying it blocks the ion-diffusion channels. This problem was solved with the newly designed cathode, which maintained a high level electron-transfer rate from the initial to the final discharge stage, as well as "open" ion-diffusion channels, as indicated in the EIS and GITT measurements.

Conclusions

In summary, to improve the rate performance of Li/CF_x primary batteries, we proposed a novel CF_x cathode design that could overcome the poor electrical conductivity and slow electrochemical kinetic problem for the inherently insulating CF_x material. By constructing a conductive network within exfoliated CF_x interlayers, the transport kinetics of electrons and ions were simultaneously improved, which was confirmed by both electrochemical and optical characterization methods. Benefiting from intimate contact between the conductive networks and CF_x flakes, together with the enlarged CF_x interlayer spacing, an enhanced rate performance of a Li/CF_x battery was observed. The design of the CF_x cathode in this work sheds light on the charge-transfer mechanism in electrochemical cells and batteries.

Author contributions

Fan Zhang: methodology, investigation, data curation, writing – original draft. Yingying Lan: methodology, data curation. Renjie Li: investigation, validation. Jianlin Wang and Yu Zhao: investigation. Shengxiang Wu: writing – review & editing. Lejuan Cai: software, validation. Wenlong Wang: conceptualization, project administration.

Conflicts of interest

There are no conflicts of interest to declare.

Acknowledgements

This work was financially supported by the Natural Science Foundation (Grant No. 21872172, 51991344, 51421002 and 22109108) of China, Chinese Academy of Sciences (Grants XDB30000000 and XDB07030100), and Guangdong Basic and Applied Basic Research Foundation (2021A1515110170).

Notes and references

1 N. Watanabe, R. Hagiwara and T. Nakajima, *J. Electrochem. Soc.*, 1984, **131**, 1980–1984.
2 N. Sharma, M. Dubois, K. Guérin, V. Pischedda and S. Radescu, *Energy Technol.*, 2021, **9**, 2000605.

3 N. Watanabe, T. Nakajima and R. Hagiwara, *J. Power Sources*, 1987, **20**, 87–92.
4 J. Read, E. Collins, B. Piekarski and S. Zhang, *J. Electrochem. Soc.*, 2011, **158**, A504.
5 Y. Ahmad, M. Dubois, K. Guérin, A. Hamwi and W. Zhang, *Carbon*, 2015, **94**, 1061–1070.
6 Q. Li, W. Xue, X. Sun, X. Yu, H. Li and L. Chen, *Energy Storage Mater.*, 2021, **38**, 482–488.
7 Z. Luo, X. Wang, D. Chen, Q. Chang, S. Xie, Z. Ma, W. Lei, J. Pan, Y. Pan and J. Huang, *ACS Appl. Mater. Interfaces*, 2021, **13**, 18809–18820.
8 Y. Li, Y. Chen, W. Feng, F. Ding and X. Liu, *J. Power Sources*, 2011, **196**, 2246–2250.
9 H. Tang, Z. Qu, Y. Yan, W. Zhang, H. Zhang, M. Zhu and O. G. Schmidt, *Mater. futures*, 2022, **1**, 022001.
10 F. Karlický and M. Otyepka, *Ann. Phys.*, 2014, **526**, 408–414.
11 H. Y. Liu, Z. F. Hou, C. H. Hu, Y. Yang and Z. Z. Zhu, *J. Phys. Chem. C*, 2012, **116**, 18193–18201.
12 Q. Zhang, S. D'Astorg, P. Xiao, X. Zhang and L. Lu, *J. Power Sources*, 2010, **195**, 2914–2917.
13 L. Li, L. Zhu, Y. Pan, W. X. Lei, Z. S. Ma, Z. Z. Li, J. J. Cheng and J. Zhou, *Int. J. Electrochem. Sci.*, 2016, **11**, 6838–6847.
14 H. Groult, C. M. Julien, A. Bahloul, S. Leclerc, E. Briot and A. Mauger, *Electrochem. Commun.*, 2011, **13**, 1074–1076.
15 G. Zhong, H. Chen, X. Huang, H. Yue and C. Lu, *Front. Chem.*, 2018, **6**, 50.
16 Y. Li, Y. Feng and W. Feng, *Electrochim. Acta*, 2013, **107**, 343–349.
17 Y. Ahmad, M. Dubois, K. Guerin, A. Hamwi and E. Flahaut, *J. Alloys Compd.*, 2017, **726**, 852–859.
18 M. Mar, M. Dubois, K. Guérin, N. Batisse, B. Simon and P. Bernard, *Carbon*, 2019, **141**, 6–15.
19 R. Jayasinghe, A. K. Thapa, R. R. Dharmasena, T. Q. Nguyen, B. K. Pradhan, H. S. Paudel, J. B. Jasinski, A. Sherehiy, M. Yoshio and G. U. Sumanasekera, *J. Power Sources*, 2014, **253**, 404–411.
20 H. P. Zhou, L. S. Yao, G. T. Chen, S. Zhang, T. T. Feng, Z. Q. Xu and M. Q. Wu, *Appl. Phys. Lett.*, 2022, **121**, 023903.
21 Q. Zhang, K. J. Takeuchi, E. S. Takeuchi and A. C. Marschilok, *Phys. Chem. Chem. Phys.*, 2015, **17**, 22504–22518.
22 G. Chen, H. Zhou, S. Zhang, Z. Zhang, T. Feng, Z. Xu and M. Wu, *ACS Appl. Energy Mater.*, 2021, **4**, 8615–8620.
23 X. Li, H. Zhang, C. Liu, J. Qiao and X. Zhou, *Microporous Mesoporous Mater.*, 2021, **310**, 110650.
24 C. Zhang and J. Lin, *Chem. Soc. Rev.*, 2012, **41**, 7938–7961.
25 Y. Jiao, R. Hu, Q. Wang, F. Fu, L. Chen, Y. Dong and Z. Lin, *Chem. - Eur. J.*, 2021, **27**, 10925–10931.
26 S. K. Bhunia, S. Nandi, R. Shikler and R. Jelinek, *Nanoscale*, 2016, **8**, 3400–3406.
27 Y. Dai, S. Cai, L. Wu, W. Yang, J. Xie, W. Wen, J.-C. Zheng and Y. Zhu, *J. Mater. Chem. A*, 2014, **2**, 20896–20901.
28 V. Gupta, T. Nakajima and B. Žemva, *J. Fluorine Chem.*, 2001, **110**, 145–151.
29 V. Lordi, P. Erhart and D. Åberg, *Phys. Rev. B*, 2010, **81**, 235204.
30 H. Xie, H. Wang, C. Fu, Y. Liu, G. J. Snyder, X. Zhao and T. Zhu, *Sci. Rep.*, 2014, **4**, 6888.
31 H. Min, D. Y. Lee, J. Kim, G. Kim, K. S. Lee, J. Kim, M. J. Paik, Y. K. Kim, K. S. Kim, M. G. Kim, T. J. Shin and S. Il Seok, *Nature*, 2021, **598**, 444–450.
32 G. Xing, N. Mathews, S. Sun, S. S. Lim, Y. M. Lam, M. Grätzel, S. Mhaisalkar and T. C. Sum, *Science*, 2013, **342**, 344–347.
33 S. D. Stranks, G. E. Eperon, G. Grancini, C. Menelaou, M. J. P. Alcocer, T. Leijtens, L. M. Herz, A. Petrozza and H. J. Snaith, *Science*, 2013, **342**, 341–344.
34 Y. Zhu, L. Zhang, H. Zhao and Y. Fu, *J. Mater. Chem. A*, 2017, **5**, 796–803.
35 S. S. Zhang, D. Foster and J. Read, *J. Power Sources*, 2009, **191**, 648–652.
36 J. Wang, M. Sun, Y. Liu, J. Lin, L. Wang, Z. Xu, W. Wang, Z. Yuan, J. Liu and X. Bai, *J. Mater. Chem. A*, 2020, **8**, 6105–6111.
37 Z. Shen, L. Cao, C. D. Rahn and C.-Y. Wang, *J. Electrochem. Soc.*, 2013, **160**, A1842–A1846.
38 P. Zhou, J. Weng, X. Liu, Y. Li, L. Wang, X. Wu, T. Zhou, J. Zhou and S. Zhuo, *J. Power Sources*, 2019, **414**, 210–217.
39 W. Weppner and R. A. Huggins, *J. Electrochem. Soc.*, 1977, **124**, 1569–1578.